

See discussions, stats, and author profiles for this publication at: <https://www.researchgate.net/publication/268872122>

First-Principles Study of the Nature of Niobium Sulfide Catalyst for Hydrodesulfurization in Hydrotreating Conditions

ARTICLE in THE JOURNAL OF PHYSICAL CHEMISTRY C · NOVEMBER 2014

Impact Factor: 4.77 · DOI: 10.1021/jp5059269

CITATION

1

READS

90

10 AUTHORS, INCLUDING:



Mauricio Cornejo

Escuela Superior Politécnica del Litoral (ESPOL)

12 PUBLICATIONS 11 CITATIONS

[SEE PROFILE](#)



Eduardo Ludena

Venezuelan Institute for Scientific Research

106 PUBLICATIONS 1,039 CITATIONS

[SEE PROFILE](#)



David Santiago Coll

Venezuelan Institute for Scientific Research

33 PUBLICATIONS 254 CITATIONS

[SEE PROFILE](#)



Cecilia Paredes

Escuela Superior Politécnica del Litoral (ESPOL)

19 PUBLICATIONS 11 CITATIONS

[SEE PROFILE](#)

First-Principles Study of the Nature of Niobium Sulfide Catalyst for Hydrodesulfurization in Hydrotreating Conditions

Yosslen Aray,^{*,†,II,‡} Dick Zambrano,[‡] Mauricio H. Cornejo,^{§,⊥} Eduardo V. Ludeña,^{†,§} Peter Iza,[‡] Alba B. Vidal,^{II} David S. Coll,^{II} Doris M. Jímenez,^{II} Francisco Henriquez,^{II} and Cecilia Paredes[⊥]

[†]Investigador Prometeo, SENESCYT, Quito, Ecuador

[‡]Facultad de Ciencias Naturales y Matemática, Departamento de Física, ESPOL, Km 30.5 via Perimetral, Campus Gustavo Galindo, Guayaquil Ecuador

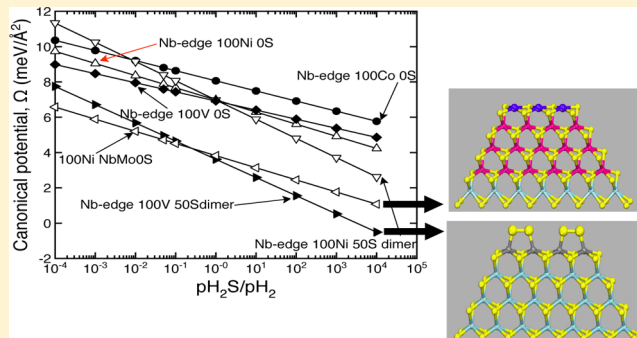
[§]Center of Nanotechnology Research and Development (CIDNA), ESPOL, Km 30.5 via Perimetral, Campus Gustavo Galindo, Guayaquil, Ecuador

^{II}Laboratorio de Físico-Química Teórica de Materiales, IVIC, Caracas, Venezuela

[⊥]Faculty of Mechanical Engineering and Production Science, ESPOL, Km 30.5 via Perimetral, Campus Gustavo Galindo, Guayaquil, Ecuador

S Supporting Information

ABSTRACT: For the metal-edge of pure NbS_2 catalyst mixed with Mo and promoted with V, Fe, Co, and Ni, density functional theory and first-principles surface thermodynamics calculations at hydrodesulfurization conditions have been performed. It was found that V, Co, and Ni promoters impart stabilization to the catalyst surfaces whereas Fe produces an opposite effect and renders the catalysts less stable. Catalyst structures corresponding to the fully Ni-promoted edge of the mixed Mo–Nb sulfide with a $\text{Mo}_3\text{Nb}_2\text{S}_{10}$ composition and to the NbS_2 V-promoted with 50% sulfur coverage forming S dimers are by far the most stable structures. The nature of the hydrodesulfurization active sites of both most stable monolayers were studied using reactivity predictors such as the electrostatic potential, the electronic localization function, and the Laplacian of the electronic density.



INTRODUCTION

There is a huge and urgent demand for ultralow-sulfur fuels to improve air quality.^{1–3} To attain this goal, transition-metal sulfides (TMS) are used as catalyst in the hydrotreatment for petroleum-based feedstock. TMS catalysts play an increasingly important role in fuel processing. The major reactions catalyzed by TMS are hydrogenation of olefins, ketones, and aromatics; hydrodesulfurization (HDS); hydrodenitrogenation (HDN); hydrodemetalation (HDM); and hydrocracking (dealkylation and ring opening of aromatics). It is also used in many other reactions including reforming, isomerization of paraffins, dehydrogenation of alcohols, Fischer–Tropsch and alcohol synthesis, hydration of olefins, amination, mercaptan and thiophene synthesis, etc.³

Nickel and cobalt promoted molybdenum sulfide catalysts, NiMoS and CoMoS , have for many years been ranked among the most important catalysts in refinery service. However, these processes and their associated catalysts, allowing the removal of sulfur, must be more and more efficient. Hence, optimization of conventional catalysts or the development of new ones is required.^{4,5}

Niobium sulfide has been reported as an interesting and affordable active phase for HDS.^{6–9} When prepared with appropriate morphology, niobium sulfides have shown promising catalytic properties. In the bulk state, they present activities higher than those of bulk MoS_2 in several model reactions,^{9–11} particularly in the thiophene HDS reaction.¹⁰ Supported together with Ni on carbon, it exhibits a high HDS activity.¹² Niobium sulfide was also used as a dopant phase to the traditional NiMoS hydrotreating catalyst and caused an enhancement in the HDS and HDN activity.¹³ In this case, niobium sulfide is presented as NbS_2 layers that are well dispersed on the support and in close contact with the other active components. Thus, NbS_2 plays the role of an additional active phase.

On the other hand, two-dimensional atom-thick layers (monolayers) have attracted much attention because of their unique applications in microscopic physics and nanoscale electronic devices.¹³ Despite their structural similarity, metal dichalcogenides present a wide variety of electronic behavior,

Received: June 14, 2014

Revised: October 28, 2014

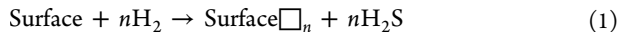
Published: November 7, 2014

going from insulators (HfS_2) to semiconductors (MoS_2) and real metals (NbS_2).^{14,15} In the case of MoS_2 , it is widely used both as a catalyst in HDS and in tribological applications.^{3,16,17} In the case of NbS_2 , it has attracted attention because of its optical, magnetic, and superconductivity properties.^{15,18} Additionally, various mixed materials have been recently synthesized,^{14,19,20} such as $\text{Nb}_x\text{Mo}_{1-x}\text{S}_2$,¹⁹ which are more stable than the corresponding pure materials.²¹

To examine the nature and stability of the monolayer of pure NbS_2 , exposing the so-called metal-edge, supporting MoS_2 sulfide and promoted by V, Fe, Co, and Ni atoms at HDS conditions, we have carried out density functional theory (DFT) calculations combined with first-principles surface thermodynamics studies. Several surface models with varying compositions have been studied.

METHODS

Thermodynamical Calculations. The variation of the surface coverage in a reactive atmosphere involving the presence of H_2 and H_2S in the gas–liquid phase in chemical equilibrium with the surface, as that present in industrial working conditions,^{22–31} would occur according to the reaction



where \square_n denotes n sulfur vacancies per unit cell. The surface stability in this environment can be determined by calculating the canonical potential $\Omega_i(T, p_i)$, at temperature T and partial pressure p_i of the gas phase components. The general thermodynamic formula for $\Omega(T, p_i)$ is

$$\Omega(T, p_i) = [G - \sum_i N_i \mu_i(T, p_i)] \quad (2)$$

where, G stands for the Gibbs free energy of the solid with a surface of area A . The solid surface is modeled by a piece of material (slab) in a grand canonical ensemble at constant temperature (T) and total pressure (P). The material slab is infinite (periodic) within the surface plane with a vacuum of 1 nm separating it from its next periodically repeated image parallel to the surface. $\mu_i(T, p_i)$ is the chemical potential of the various species i present in the system, and N_i gives the number of atoms of the i th component contained in the solid slab model. For the NbS_2 surfaces, eq 2 can be written as

$$\Omega(T, p_i) = [G_{\text{NbS}_2}^{\text{slab}} - N_{\text{Nb}} \mu_{\text{Nb}}(T, p) - N_{\text{S}} \mu_{\text{S}}(T, p)] \quad (3)$$

where $G_{\text{NbS}_2}^{\text{slab}}$ stands for the total Gibbs free energy of the slab and μ_{Nb} and μ_{S} are the chemical potentials of a Nb atom and a S atom, respectively. Under chemical equilibrium, μ_{S} is the same in all phases that are in contact and contain sulfur. Hence, the following relationships between bulk NbS_2 and its components are satisfied:

$$\mu_{\text{Nb}} + 2\mu_{\text{S}} = \mu_{\text{NbS}_2}(\text{bulk}) \quad (4)$$

If there is enough bulk material to act as a thermodynamic reservoir, the potentials are related by the Gibbs free energy of the bulk sulfide

$$\mu_{\text{Nb}} + 2\mu_{\text{S}} = G_{\text{NbS}_2}(\text{bulk}) \quad (5)$$

Hence, the chemical potential of Nb in the surface energy expression $\Omega(T, p_i)$ is equal to the corresponding chemical potential of Nb in the bulk phase

$$\mu_{\text{Nb}} = G_{\text{NbS}_2}(\text{bulk}) - 2\mu_{\text{S}} \quad (6)$$

Combining eqs 3 and 6, the temperature dependence of the surface Gibbs free energy enters only through the chemical potentials of the gases in contact with the surface



$$\mu_{\text{S}} = \mu_{\text{H}_2\text{S}} - \mu_{\text{H}_2} \quad (8)$$

$$\Omega(T, p) = [G_{\text{NbS}_2}^{\text{slab}} - N_{\text{Nb}} G_{\text{NbS}_2}(\text{bulk})] - \frac{1}{2} \Gamma_S \mu_{\text{S}}(T, p) \quad (9)$$

$$\Gamma_S = \frac{1}{A} (N_{\text{S}} - 2N_{\text{Nb}}) \quad (9)$$

Γ_S is the surface sulfur excess with respect to a stoichiometric surface termination. Equation 9 has been generalized by Finnis³² for polar interfaces (e.g., grain boundary or solid surface) in multicomponent systems and has been used by numerous authors in the literature to calculate and compare the surface energy for different terminations for polar oxide and for transition-metal sulfide surfaces.^{22–25}

The Gibbs free energy is associated with the Helmholtz free energy, F , via³³

$$G(T, p, N_{\text{Nb}}, N_{\text{S}}) = F(T, p, N_{\text{Nb}}, N_{\text{S}}) + pV(T, p, N_{\text{Nb}}, N_{\text{S}}) \quad (10)$$

In general, the Helmholtz free energy can be written as

$$F(T, V, N_{\text{Nb}}, N_{\text{S}}) = E_{\text{DFT}}^{\text{total}}(V, N_{\text{Nb}}, N_{\text{S}}) + F^{\text{vib}}(T, V, N_{\text{Nb}}, N_{\text{S}}) \quad (11)$$

with

$$F^{\text{vib}}(T, V, N_{\text{Nb}}, N_{\text{S}}) = E^{\text{vib}}(T, V, N_{\text{Nb}}, N_{\text{S}}) - TS^{\text{vib}}(T, V, N_{\text{Nb}}, N_{\text{S}}) \quad (12)$$

comprising all contributions, which depend on vibrational modes in the system. Here, E^{vib} and S^{vib} are the vibrational energy (including the zero-point energy) and entropy, respectively. The pV term is negligible^{32–34} ($\sim 10^{-3}$ meV/ \AA^2) compared to the F free energy, which is of the order of tenths of millielectronvolts per square angstrom. Thus, the only additional contributions to G apart from the DFT total energy are the vibrational terms

$$E^{\text{vib}} = \frac{R}{k} \frac{1}{2} \sum_i \frac{(hv_i) \exp(-hv_i/kT)}{[1 - \exp(-hv_i/kT)]} \quad (13)$$

$$S^{\text{vib}} = R \sum_i \frac{(-hv_i/kT) \exp(-hv_i/kT)}{[1 - \exp(-hv_i/kT)]} - R \sum_i \ln[1 - \exp(-hv_i/kT)] \quad (14)$$

Typically, vibrational contributions to differences in the Gibbs free energies of extended systems exhibit some cancellation.^{32–34} If F^{vib} were completely negligible, leaving only the DFT energy as the G predominant term, eq 9 would be written as

$$\Omega(T, p) = [E_{\text{NbS}_2}^{\text{slab}} - N_{\text{Nb}} E_{\text{NbS}_2}(\text{bulk})] - \frac{1}{2} \Gamma_S \mu_{\text{S}}(T, p) \quad (15)$$

which contains exclusively terms directly obtainable from a DFT calculation. For RuO_2 ,³³ PdO ,³⁵ and Cu_2O ³⁶ surfaces, rough estimation of the vibrational contribution showed that this stays

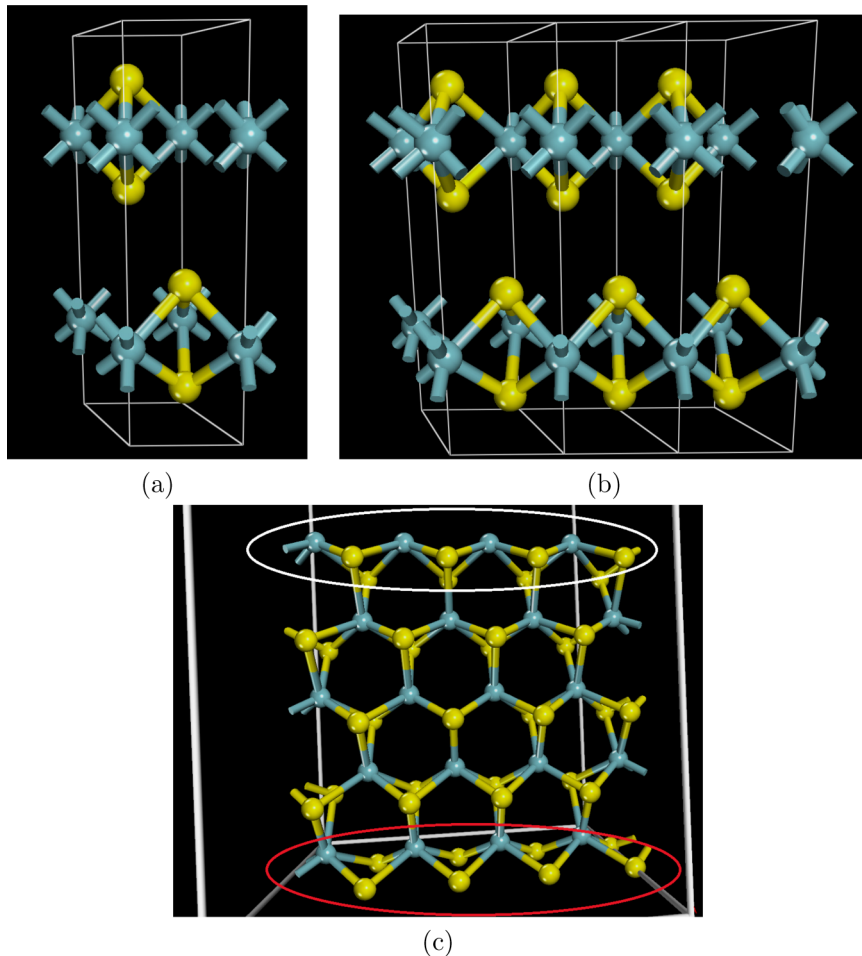


Figure 1. (a) Ball and stick model of the unit cells (white lines) of the NbS₂ bulk. (b) Expansion of three periodic cells showing two NbS₂ monolayers. (c) Unit cell of the monolayer model showing the Nb-edge (highlighted by a white circle) and the S-edge (highlighted by a red circle). Yellow and blue spheres denote the S and Nb atoms, respectively. Cleaving perpendicular to the layers produces the (100) surface models show in panel c.

below 10, 20, and 5 meV/Å² in the whole temperature range considered, respectively. Such a 10 meV/Å² contribution is certainly not a completely negligible factor; however, it was considered that this uncertainty does not affect any of the physical conclusions drawn with respect to the applications studied. In the same way, MoS₂ surface studies have also neglected this factor.^{22–26,34} Recently, reduction pathways of MoS₂ edges by hydrogen including entropic and enthalpy corrections to electronic energies deduced from the sets of vibrational frequencies for the gas phase and catalytic edges have been reported.³⁷ Significant corrections on the activation free energies and on the stabilities of the intermediate states were found. In the present work, we include the vibrational contribution for all studied surface models, bulk models, and H₂S and H₂ molecules needed at eqs 12 to 17 and perform a full vibrational calculation using the standard methodology implemented in the program Dmol³.^{38–40}

In practical calculations, the chemical potential of the gas-phase mixture (H₂ + H₂S) is evaluated using the general thermodynamic formula assuming ideal gas behavior

$$\mu_s(T) = \Delta E_{el} + \Delta ZPE + \Delta H(T) - T\Delta S(T) + RT\ln\left(\frac{p_{H_2}S}{p_{H_2}}\right) \quad (16)$$

where $\Delta H(T)$ and $\Delta S(T)$ stand for enthalpy and entropy differences, respectively, at T for H₂S and H₂ and ΔE_{el} for the difference of their internal energies ($E_{el}(H_2S) - E_{el}(H_2)$), which are approximated by their zero-temperature DFT total energies. ΔZPE represents the zero-point vibrational energy term $H_{H_2S}(0) - E_{el}(H_2S) - (H_H(0) - E_{el}(H_2))$ calculated through evaluation of the Hessian matrix elements using the normal modes analysis module implemented in the program Dmol³.^{38–40}

Large values of μ_s correspond to sulfur-rich conditions, whereas small values of μ_s relate to strongly reducing conditions in which hydrogen is more abundant than H₂S in the gas phase.

For surface promoted with Me atoms (V, Fe, Ni, Co) and with composition Nb_xMe_yS_z the canonical potential is given by

$$\Omega(T, p) = \left[G_{Nb_xMe_yS_z}^{\text{slab}} - xG_{NbS_2}(\text{bulk}) - \frac{y}{b}G_{MeBSc}(\text{bulk}) \right] - \Gamma_S\mu_s(T, p) \quad (17)$$

$$\Gamma_S = \left(z - xa - y\frac{c}{b} \right)$$

where Me_bS_c is the promoter reference bulk-phase stable (VS, FeS₂, Ni₃S₂, Co₉S₈) in reaction conditions.

For example, for Co atom as promoter, Ω is given by

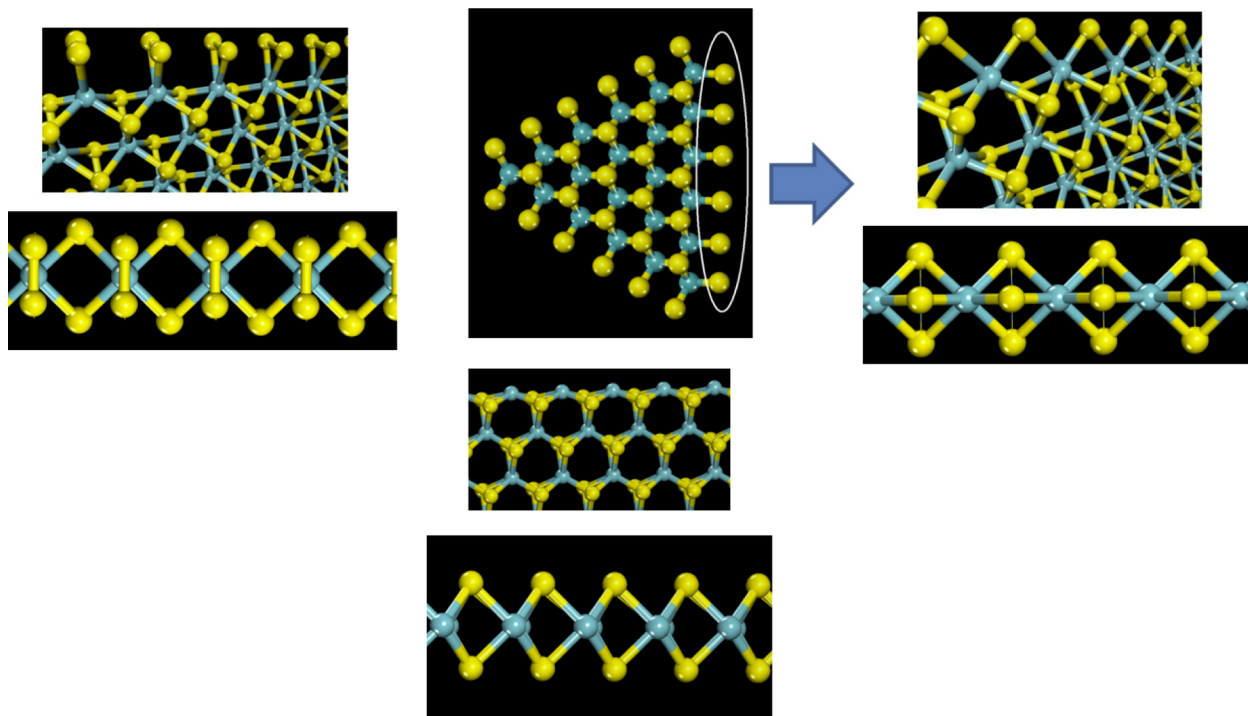


Figure 2. Ball and stick model of a single-layer NbS₂ nanoparticle (center). A white circle highlights one edge of the particle. Yellow and blue spheres denote the S and Nb atoms, respectively. (Left-hand panels) Atomic structure of the fully sulfide Nb-edge with 100% of sulfur coverage. Note the presence of exposed S₂-dimer. (Right-hand panels) Atomic structure of the Nb-edge with 50% of S coverage with outermost S atoms in bridging Nb–Nb position. (Bottom panels) Atomic structure of the Nb-edge with 0% sulfur coverage. For each case, top and bottom panels show side- and top-view of the model.

$$\Omega(T, p) = \left[G_{\text{CoMoS}}^{\text{slab}} - xG_{\text{NbS}_2}(\text{bulk}) - \frac{y}{9}G_{\text{Co}_9\text{S}_8}(\text{bulk}) \right] - \frac{1}{2}\Gamma_S\mu_S(T, p)$$

$$\Gamma_S = \left(z - 2x - \frac{8}{9}y \right) \quad (18)$$

Surfaces Models. NbS₂ has a lamellar structure similar to that of MoS₂ bulk (see Figure 1).⁴¹ In the unit cell, locally six sulfur atoms are coordinated to one Nb atom to form a trigonal prismatic arrangement.⁴¹ Each Nb atom is surrounded by six first-nearest sulfur atoms at a distance of 2.843 Å forming a NbS₂ sheet (a monolayer), while each S atom is surrounded by three first-nearest Nb atoms on the sheet and by three second-nearest S atoms located on a neighbor NbS₂ monolayer. Cleavage of the bulk structure parallel to the {100} plane produces the edge surface models exposing coordinatively unsaturated molybdenum or sulfur atoms (see Figure 1c). Such a model of a single layer exposes simultaneously the two well-known kinds of MoS₂-like catalysts edges: the M-edge at the top of Figure 1c (highlighted by a white circle) and the S-edge at the bottom (highlighted by a red circle). We have just studied the so-called metallic M-edge. Figure 2 shows the sulfur coverage for the periodic models of the Nb-edges used in the present work. Our monolayer model exhibits five NbS₂ rows (similar to the highlighted rows in Figure 1c) in the *z* direction perpendicular to the surface. The periodicity in the *x* direction along the edges of the sheets in four Nb–Nb distances (4 × 1 supercell) so that four nonequivalent Nb surfaces sites are present. The Nb-edges are fully saturated (100% coverage) when the outermost four Nb

atoms are bonded to eight outermost sulfur atoms, i.e., two by Nb atoms (left of Figure 2). The coverage is decreased by removing atoms from the edge. When four S atoms are removed, we have the edge with 50% of coverage (right of Figure 2). In this case, the Nb edges contain two S atoms per cell located in the bridging position in-plane with the Nb atoms forming S monomers; while the model with 0% coverage contains four nude coordinated metallic atoms.

Promotion by means of substitution of Nb atoms at the edge by V, Fe, Co, and Ni was also studied. A very large number of local configurations, sulfur coverage, and distribution of promoters can be studied. However, we have just investigated the most stable models (see Figure 3) as reported by previous DFT calculations (Schweiger et al.²³) for the MoS₂ monolayer promoted with Ni and Co atoms: 100% promoted, with 0% S coverage (Figure 3a); with 50% S coverage in bridge configuration (Figure 3b); with 50% S coverage forming S–S dimers (Figure 3c); and 50% promotion in alternated configuration with 25% S coverage (Figure 3d).

DFT Calculations. All total energy calculations were performed by means of the DMol³^{38–40} program using the Kohn–Sham Hamiltonian with the gradient-corrected Perdew–Becke–Ermzerhof (PBE) exchange-correlation functional.⁴² DMol³ calculates variational self-consistent solutions to the DFT equations, expressing numerically the atomic orbital basis functions in an accurate spherical-polar mesh. The solutions to these equations provide the molecular electron densities, which can be used to evaluate the total electrostatic potential of the system. The numerical double- ζ plus polarization basis set DNP³⁸ was used in all calculations. DMol³ uses a numerical basis set within DFT to obtain high accuracy while maintaining a computational cost that is relatively low compared to that of

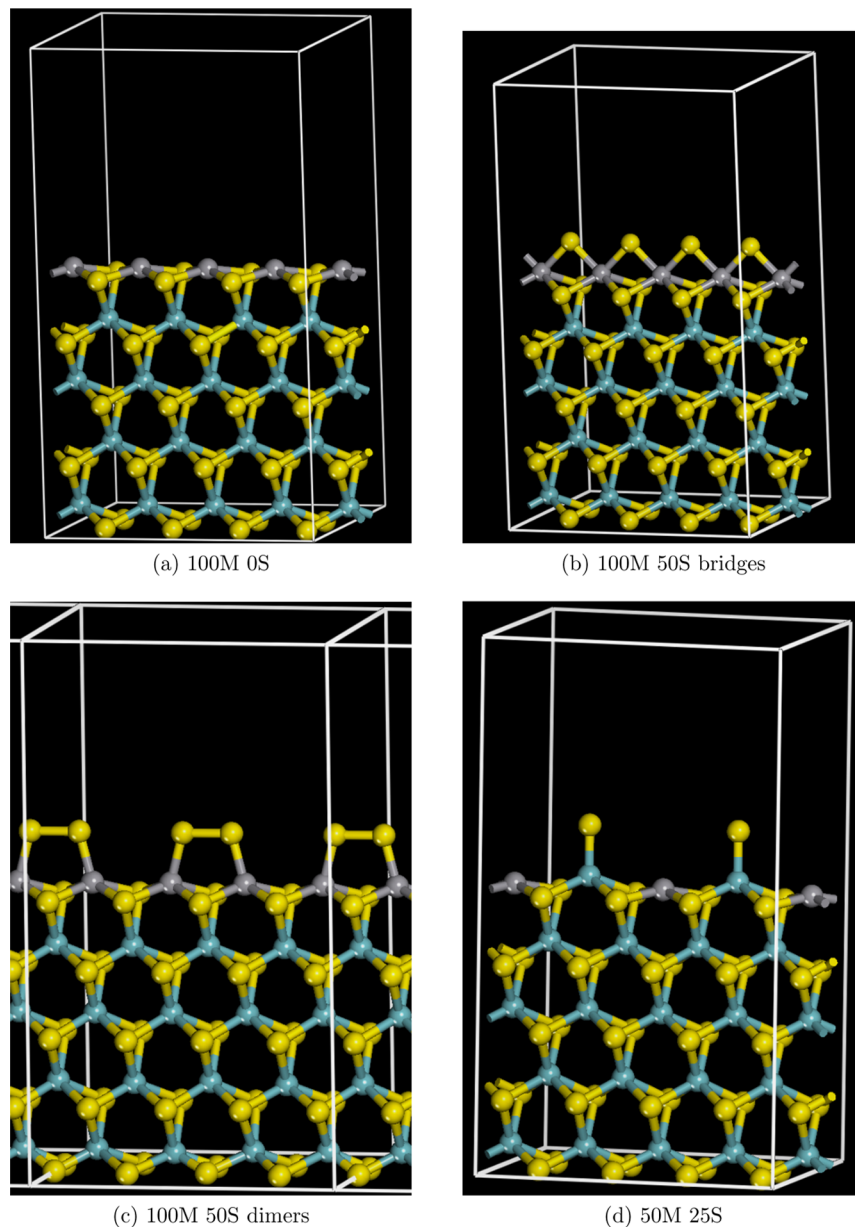


Figure 3. Geometries of the MNbS metal edge ($M = V, Fe, Co, Ni$) for (a) 100% promotion and 0% sulfur coverage, (b) 100% promotion and 50% S coverage forming bridges, (c) 100% promotion and 50% forming dimers, and (d) 50% promotion and 25 S coverage. Gray, light blue, and yellow spheres denote M, Nb, and S atoms, respectively.

other ab initio methods. We have modeled all surfaces using periodic slabs with atoms initially located at their ab initio bulk positions. Vacuum layers thicker than 15 Å were used to ensure that there were no interactions between adjacent slabs. The geometry of those models was optimized using algorithms included in the DMol³ program.

RESULTS AND DISCUSSION

Thermodynamic Stability for Nonpromoted Nb and Mo Sulfide Monolayers. To determine the stability of the studied surfaces at HDS conditions, their canonical potentials, Ω , were calculated using 9, 15, 17, and 18. In Figure 4, plots of Ω as a function of the pH₂S/pH₂ ratios at 650 K are presented for the NbS₂ monolayer models. At a given pressure ratio, the lower the surface energy, the more stable the corresponding surface model. Except for the stoichiometric surface (0% coverage), the other

surface terminations are more stable (negative slope) as the pH₂S/pH₂ ratio (and pH₂S) increases. The monolayer with 50% sulfur coverage is the most stable one over the whole pressure range. For very strong sulfiding conditions ($pH_2S/pH_2 > 500$), 100% and 50% coverage are relevant and compete in stability. At HDS conditions ($0.01 \geq pH_2S/pH_2 \leq 0.05$) the NbS₂ monolayer with 50% S coverage is by far more stable than surfaces with 100% coverage. This follows the same trend reported for MoS₂ multilayers case.²¹ Nevertheless, a few differences at strong sulfiding conditions were observed. Therefore, we have performed a similar study for similar MoS₂ monolayers, and the results are shown in Figure 5. For MoS₂, there is an intersection point between the stability lines of 50% and 100% S coverage at $pH_2S/pH_2 = 1000$. Above this value, corresponding to high H₂S pressure, the 100% coverage is the most stable state. For NbS₂, the monolayer with 50% coverage is the most stable configuration in the whole pH₂S/pH₂ range studied. These

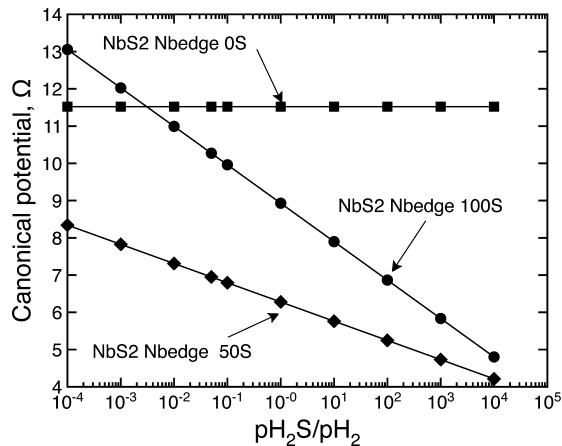


Figure 4. Variation of the canonical potential, $\Omega(T, \text{pH}_2\text{S}/\text{pH}_2)$, as a function of the $\text{pH}_2\text{S}/\text{pH}_2$ ratio at 650 K for the studied NbS_2 surfaces. Each line is labeled by the corresponding sulfur coverage. In the plot, a pressure range of $10^{-4} < \text{pH}_2\text{S}/\text{pH}_2 < 10^4$ is used, corresponding to the stability of the NbS_2 phases.

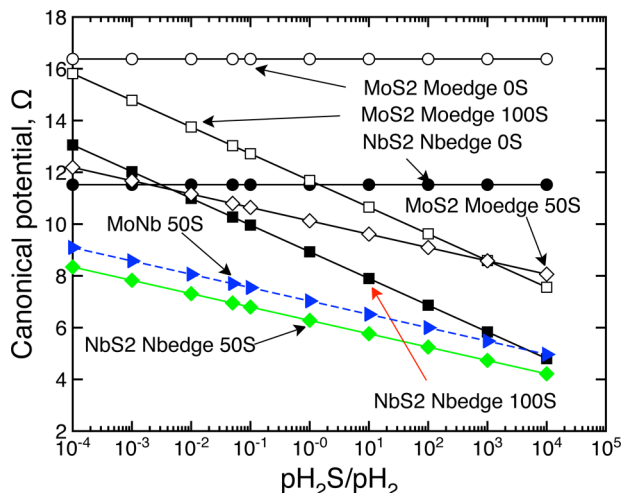


Figure 5. Variation of the canonical potential, $\Omega(T, \text{pH}_2\text{S}/\text{pH}_2)$, as a function of the $\text{pH}_2\text{S}/\text{pH}_2$ ratio at 650 K for the MoS_2 , NbS_2 and mixed studied surfaces. Each line is labeled by the corresponding sulfur-coverage. In the plot, a pressure range $10^{-4} < \text{pH}_2\text{S}/\text{pH}_2 < 10^4$ is used, corresponding to the stability of the NbS_2 phases. Green and blue lines denote the most stable monolayers among pure phases and Mo-Nb mixed monolayers, respectively.

results suggest that at 600 K the affinity of the S-dimers on top of the Nb-edge is smaller than those on the top of Mo-edge. However, for both catalysts, in order for the metal-edge with 100% S coverage to compete in stability with the 50% S coverage a very strong sulfiding environment is required. Interestingly, in Figure 5 it can be seen that the NbS_2 monolayers are systematically more stable than the corresponding surfaces of MoS_2 . Similar results have been reported²¹ for the Mo → Nb substitution on MoS_2 nanotubes using the density functional tight-binding method. It was found that composite $\text{Mo}_{1-x}\text{Nb}_x\text{S}_2$ nanotubes (with Nb contents of 5, 10, and 25%) are more stable than the corresponding pure Mo tubes. In the same way, ab initio studies of mixed molybdenum–niobium disulfides have shown that for Nb doping of MoS_2 up to 25% the substitutional process is exothermic.¹⁴ For these materials, Nb doping causes a transition from semiconductor behavior in MoS_2 to metallic performance in the mixed sulfide. In the present paper, we have

constructed a mixed Mo–Nb monolayer with $\text{Mo}_3\text{Nb}_2\text{S}_{10}$ composition by substitution of the three upper rows of Nb atoms in the Nb_50S model with Mo atoms (see Figure 6). This

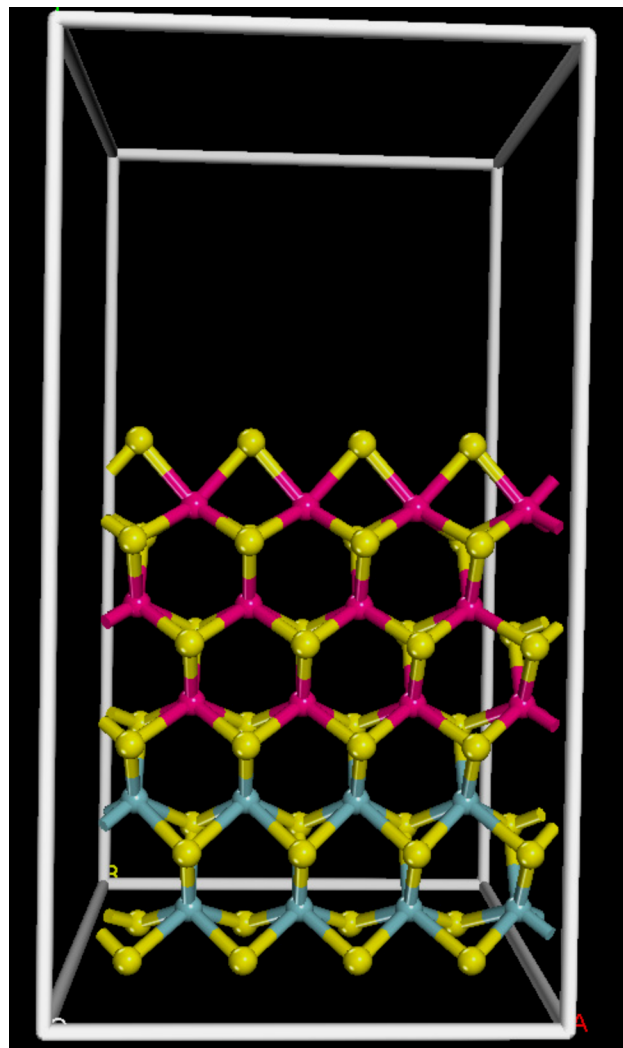


Figure 6. Ball and stick model of mixed MoNb 50S exposing 50% S coverage at the Mo-edge. Yellow, pink, and blue spheres denote S, Mo, and Nb atoms, respectively.

mixed monolayer can be considered to be a simple model of molybdenum sulfide supported on niobium sulfide. The geometry of this model was optimized, and the canonical potential was calculated and also plotted in Figure 5. The Mo_50S surface is appreciably stabilized for the effect of the Nb atoms, and it is more stable than all pure MoS_2 surface models over the entire range of pressure ratios and very close to the Nb_50S surface. This result agrees with the reports about the use of niobium sulfide as a dopant phase in the traditional NiMo hydrotreating catalysis¹² where it is indicated that niobium is present as NbS_2 layers, well-dispersed on the support, and in close contact with the other active components. $\text{Nb}_2\text{Mo}_3\text{S}_{10}$ ^{7,19} was prepared and studied, and formation of mixed lamellar sulfide was proven, but it is not clear whether the intralayer or the interlayer mixed phase was obtained. In any case, the present result suggests that the presence of niobium in molybdenum sulfide stabilizes the catalysts. At this point, it is interesting to check the thermal and entropic impacts on the stability diagrams

of Figures 4 and 5. Therefore, the values of Ω without and including the F^{vib} term for the NbS_2 , MoS_2 , and mixed monolayer models used in those figures were reported in Table S1 of Supporting Information. These values were calculated for reducing conditions ($\text{pH}_2\text{S}/\text{pH}_2 < 1.0$) comprising the typical HDS conditions ($\text{pH}_2\text{S}/\text{pH}_2 = 0.05$) and high H_2 pressure. It can be deduced that vibrational corrections 650 K decrease the canonical potential for 2.199, 2.023, 1.055, 1.230, 1.061, 1.027, and 0.891 eV for $\text{NbS}_2\text{-100S}$, $\text{NbS}_2\text{-50S}$, $\text{NbS}_2\text{-0S}$, $\text{MoS}_2\text{-100S}$, $\text{MoS}_2\text{-50S}$, $\text{MoS}_2\text{-0S}$, and $\text{MoNb}\text{-50S}$ monolayers, respectively. These values mean differences at $\text{pH}_2\text{S}/\text{pH}_2 = 0.05$ ranging from 23–18% for 100% S coverage to 6–9% for 0% S coverage. However, we have observed that the tendency of the thermodynamic stability of the models studied generally remains very similar. A similar conclusion was reported for RuO_2 surfaces;³³ nevertheless, it was stressed that is not a general result and there might be applications in which the inclusion of the vibrational contribution can be critical.³³

Promotion Effects. To explore the affinity of the promoter for the studied Nb-edge models (Figure 3), we have plotted in Figure 7 diagrams for Ω showing the effect of doping with V, Fe,

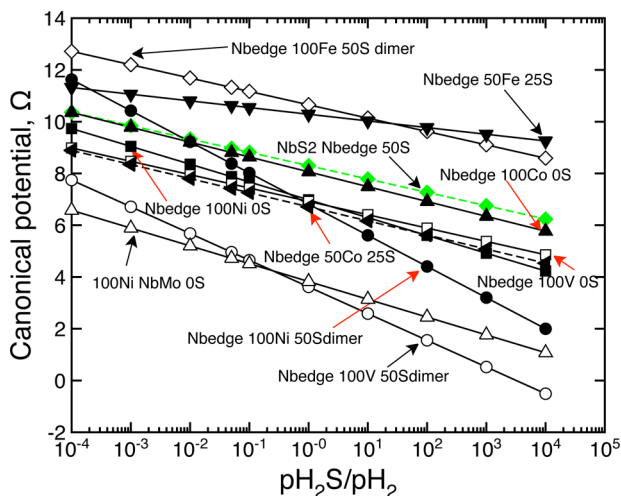


Figure 7. Effect of promotion on the NbS_2 surface stability.

Co, and Ni. Partial substitution (Figure 3d) was also explored. In contrast to the reported results for MoS_2 edged,²⁴ we observed that partial promoter substitution reduced the energy of the metal-edge only for Fe and Co monolayers. Thus, only for these two cases, partial promotion is reported in Figure 7. This picture shows that Ni, Co, and V promoters impart stabilization to the catalyst surfaces: lower γ values than the $\text{NbS}_2\text{-50S}$ surface for all the studied Ni, Co, and V cases; while Fe produces an opposite effect as they render the catalysts less stable: all the monolayer models for Fe show bigger values of Ω than the $\text{NbS}_2\text{-50S}$ case. For V, Fe, and Co the most stable monolayer correspond to the 100% promoted with 50% S coverage and the S atoms forming dimers (See Figure 3c) while for Ni, the most stable one is also 100% promoted but with 0% S coverage (Figure 3b). The fully promoted metal-edge with Ni of the mixed Mo–Nb ($100\text{Ni}\text{-MoNb}\text{-0S}$) and of the vanadium with 50% S coverage forming dimer (100V-50Sdimer) surfaces are the most stable ones over the whole range of pressure. The vanadium surface becomes more stable as the sulfiding conditions increase ($\text{pH}_2\text{S}/\text{pH}_2 > 10$) while for reducing regime ($\text{pH}_2\text{S}/\text{pH}_2 < 0.01$), the $100\text{Ni}\text{-MoNb}\text{-0S}$ monolayer tends to be the most stable. The

intersection place occurs at $\text{pH}_2\text{S}/\text{pH}_2 = 0.5$. Around the HDS typical condition ($\text{pH}_2\text{S}/\text{pH}_2 = 0.05$) both surfaces have similar stabilities (See Figure 7 and Table S2 of Supporting Information). At this point, the mixed monolayer containing Ni is 4.25 eV more stable than the pure NbS_2 with 50% S. The next set in stability comprises the Co and Ni promoter monolayers. Increase of the partial pressure of H_2S to $\text{pH}_2\text{S}/\text{pH}_2 > 10$ enhances the stability of 100Co-50S dimers while for reducing conditions ($\text{pH}_2\text{S}/\text{pH}_2 < 1$) the partial promoted 50Co-25S model is the most stable of the set. A similar result was reported for MoS_2 monolayer.²⁴ In particular for usual HDS conditions, $\text{pH}_2\text{S}/\text{pH}_2 = 0.05$, the 50Co-25S , 100Ni-0S and 100Co-50Sdimer are 1.552, 1.095, and 0.579 eV more stable (See Table S2 of Supporting Information) respect the most stable of the pure NbS_2 monolayer: $\text{NbS}_2\text{-50S}$. The partial promoter 50Fe-25S is the most stable of Fe monolayers for $\text{pH}_2\text{S}/\text{pH}_2 < 50$, involving strong sulfiding and reducing conditions, while the 100Fe-50Sdimer is the most stable one for very strong sulfiding conditions ($\text{pH}_2\text{S}/\text{pH}_2 > 50$). For typical HDS conditions (See Table S2 of Supporting Information), 50Fe-25S and 100Fe-50Sdimer are 1.652 and 2.352 eV least stable than the pure $\text{NbS}_2\text{-50S}$ monolayer. Thus, at HDS conditions, the obtained tendency of thermodynamics stability for the studied monolayers is $100\text{Ni-MoNb-0S} > 100\text{V-50Sdimer} > 50\text{Co-25S} > 100\text{Ni-0S} > \text{Nbedge-50S} > 50\text{Fe-50S}$. In summary, we observed that the monolayer model with $\text{Mo}_3\text{NbNiS}_{10}$ composition is by far more stable at HDS conditions than pure NbS_2 monolayer even with Co, Ni, and Fe promotion. 100Ni-MoNb-0S monolayer is 2.7, 3.16, 4.25, and 5.90 eV more stable than the 50Co-25S , 100Ni-0S , Nbedge-50S , and the 50Fe-25S monolayers, respectively.

Nature of the Active Sites. To investigate the nature of the HDS active sites of both most stable monolayers, we have resorted to reactivity predictor criteria like electrostatic potential,^{30,31,43,44} $V(\mathbf{r})$, electronic localization function,^{45,46} electron localization function (ELF), and the Laplacian of the electronic density.^{47–51} For surfaces exposing metal atoms, such as the 100Ni-MoNb-0S surface, an interesting way to visualize and quantify the Lewis acid strength of the active sites is simply to map the electrostatic potential $V(\mathbf{r})$ on the $\rho(\mathbf{r}) = 0.001$ isocontour.^{43,44} Such a mapping allows us to identify the host sites in which nucleophiles (most positive zone) and electrophiles (most negative zone) should bind. Additionally, the local maximum value of $V(\mathbf{r})$, V_{\max} at the determined host zones provides a quantitative determination of the Lewis acidity strength on the outermost atoms. Figure 8 shows this mapping for the mixed catalysts surface; starting from the most negative $V(\mathbf{r})$ values (see caption of Figure 8), three different tones of the blue and three of green are used to represent the range of the most negative $V(\mathbf{r})$ values while two yellow tones, one orange, one brown, one purple, two red tones, one white, and one gray denote the positive $V(\mathbf{r})$ values. As expected, the most positive zones are localized right at the top of the exposed Ni atoms; a red zone containing a local maximum value of 118.479 kJ/mol which is bigger than the corresponding value for MoS_2 (58.86 kJ/mol) but lower than that of RuS_2 (181.16 kJ/mol),^{30,42} a very active catalysts. $V(\mathbf{r})$ suggests the presence of strong Lewis acid sites at the border of the monolayer. In order to easily see this feature, we have plotted in Figure 8b a contour map of $V(\mathbf{r})$ at the plane containing all the metal atoms. This picture shows how the positive zone of the Ni atoms (indicated by blue arrows) is exposed to the incoming molecules containing the contaminant sulfur atoms. Additionally, we also provide an ELF plot in Figure

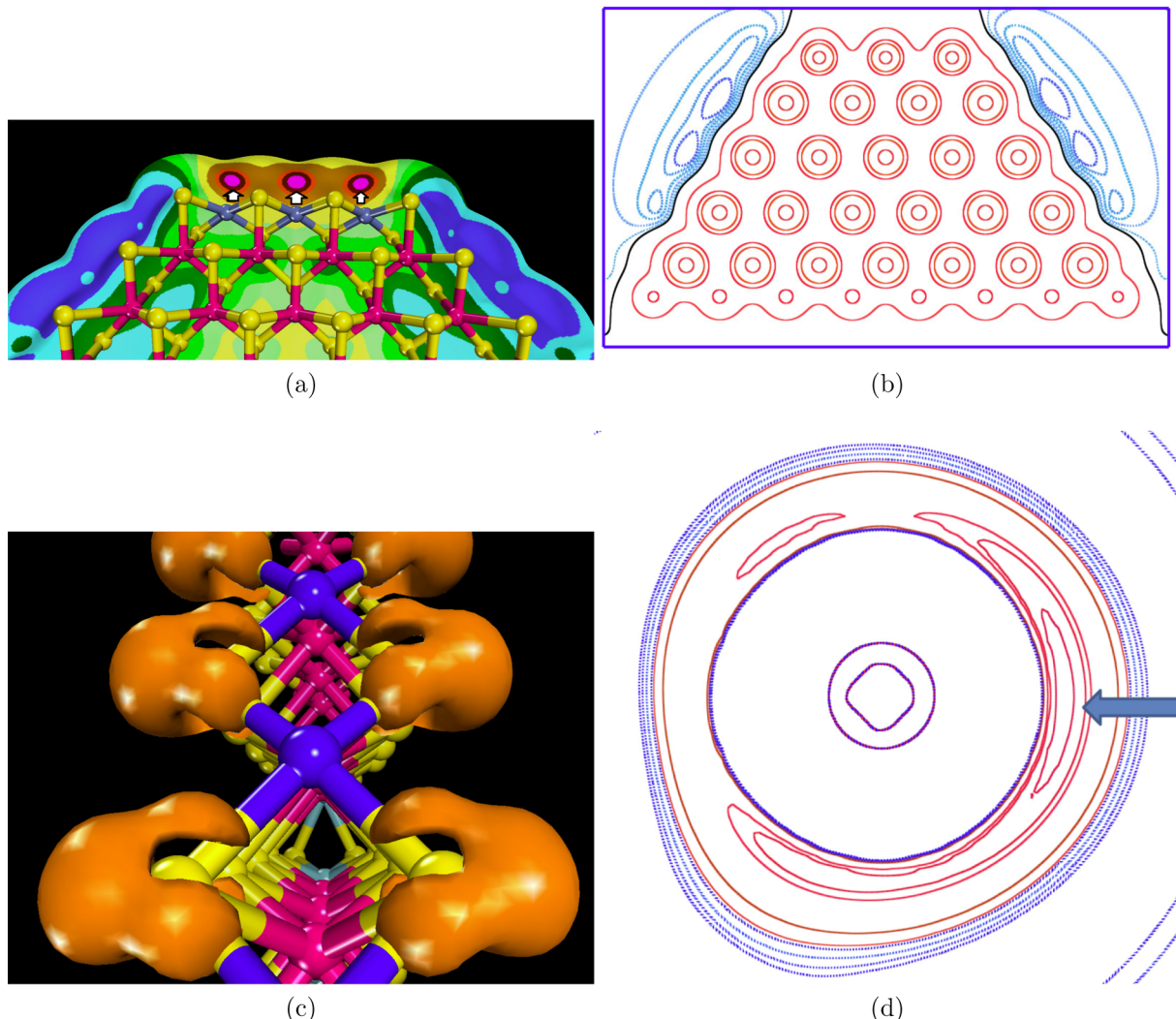


Figure 8. (a) Electrostatic potential $V(r)$ color mapped on the cap of the $\rho(r) = 0.001$ contour for the mixed MoNb OS monolayer. The tab at the bottom is blue jay (−157.530 to 78.765 kJ/mol), blue heaven (−78.765 to 42.008 kJ/mol), light blue (−42.008 to −31.506 kJ/mol), dark green (−31.506 to −21.004 kJ/mol), green (−21.004 to −10.502 kJ/mol), light green (−10.502 to 0.000 kJ/mol), light yellow (0.000 to 26.255 kJ/mol), yellow cream (26.255 to 52.510 kJ/mol), orange (52.510 to 65.638 kJ/mol), brown (65.638 to 78.765 kJ/mol), purple (78.765 to 91.893 kJ/mol), light red (91.893 to 105.020 kJ/mol), red (105.020 to 144.403 kJ/mol), white (144.403 to 183.75 kJ/mol), and gray (185.75 to 236.295 kJ/mol). (b) Contour map $V(r)$ just at the plane containing all the metal atoms. Blue and red contours denote the negative and positive value of the electrostatic potential. Arrows point to the Ni active sites. (c) Isocontour map of ELF showing the ELF = 0.7 localization domain. (d) Contour map of the $\nabla^2\rho$ for one of the S atoms shown in panel c and in a plane perpendicular to the picture in panel c. A blue arrow points to the exposed S lone pair.

8c. ELF associates the localization of an electron with the probability density for finding a second like-spin electron near the reference point.⁴⁵ ELF gives an idea of where the electrons are localized. In agreement with the electrostatic potential analysis, it can be seen that for the Nb-edge of the 100Ni_MoNb_OS monolayer, the electrons are localized around the S atoms that are coordinated to the Ni atoms. Finally, a Laplacian of the $\rho(r)$ map for one of those S atoms is shown in Figure 8d. Note the presence of a local charge concentration such as the well-known “banana” type, which is characteristic of the Lewis lone pair.^{47,49,50} The Laplacian determines the regions of space in which the electronic charge is locally concentrated or depleted.^{47–51} Wherever the Laplacian of ρ is negative (red contour in Figure 8d), there is a local concentration of charge, that is, the electronic density is greater than the average density in the immediate neighborhood. Wherever the Laplacian is positive, there is an analogous local depletion of charge. The localized concentrations of charge mimic the pairs of electrons assumed in

the Lewis model in number, relative position, and size.⁴⁹ The local charge concentration shown in Figure 9c is located outside the monolayer and corresponds to the site where electrons are available for attaching with atoms such as hydrogen and forming S–H groups.

For the 100 V_50Sdimer monolayer, panels a and b of Figure 9 present its geometry and an isocontour map of ELF showing the ELF = 0.7 localization domain, respectively. Note that the electrons are localized around the S atoms, hindering the access to the metal atoms. Additionally, Figure 9c displays the Laplacian contour map just for the S_2 dimer located on the Nb-edge. This map shows the presence of local charge concentration exposed outside the surface. These local concentrations are available to link hydrogen atoms and form SH groups.

At this point we stress that very important kinetic aspects are not considered in this reactivity predictor approach and a more in-depth study of the pathways, transition states, and activation energies of the elementary reaction involved in the DDS and

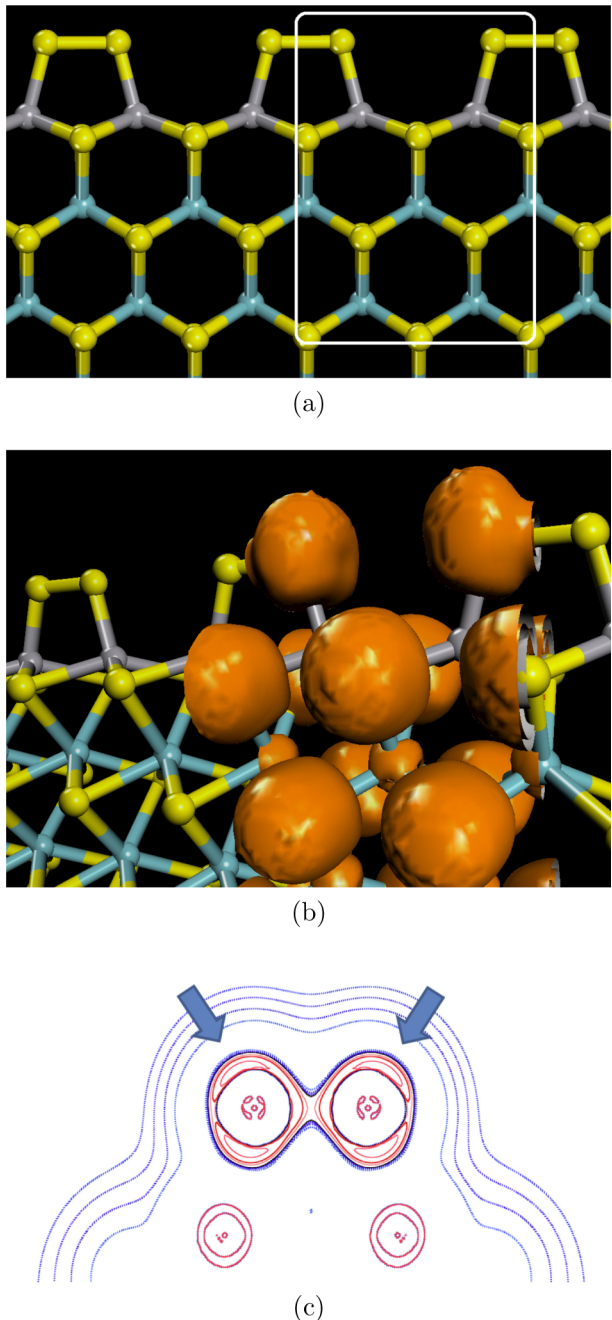


Figure 9. (a) Ball and stick model of the 100 V 50Sdimer monolayer. Yellow, light pink, and light blue denote the S, V, and Nb atoms, respectively. A white square highlights the zone where ELF is plotted in panel b. (b) Isocontour map of ELF showing the ELF = 0.7 localization domain. (c) Contour map of the $\nabla^2 \rho$ for one of the S dimers in the plane of the picture. Arrows point to the exposed sulfur lone pairs.

HYD routes must still be promoted. Studies of these aspects are currently underway in our lab.

CONCLUSIONS

Combination of DFT and first-principles surfaces thermodynamics studies of the metal-edge of pure NbS_2 mixed with Mo and promoted with V, Fe, Co, and Ni have shown that at HDS conditions, in general, Ni, Co, and V promoters impart stabilization to the catalysts surfaces. On the other hand, Fe produces the opposite effect by making the catalysts less stable.

However, the fully promoted edge with Ni of the mixed Mo–Nb sulfide with $\text{Mo}_3\text{Nb}_2\text{S}_{10}$ composition and the NbS_2 V-promoted with 50% sulfur coverage forming dimers surfaces are by far the most stable ones. The nature of the HDS active sites of the two most stable monolayers were studied by means of reactivity predictor criteria such as the electrostatic potential, $V(\mathbf{r})$, the electronic localization function, ELF, and the Laplacian of the electronic density.

ASSOCIATED CONTENT

Supporting Information

Thermodynamic corrections to the canonical potential for the NbS_2 , MoS_2 , and mixed sulfur monolayer models (Table S1); canonical potential for each model plotted in Figure 7 and difference with respect to the Nedge_50S monolayer value at $\text{pH}_2\text{S}/\text{pH}_2 = 0.05$ (Table S2). This material is available free of charge via the Internet at <http://pubs.acs.org>.

AUTHOR INFORMATION

Corresponding Author

*E-mail: yaray@espol.edu.ec.

Notes

The authors declare no competing financial interest.

ACKNOWLEDGMENTS

We thank Dr. Javier Torres for providing some of the computational resources and for performing the vibrational calculations used in Tables S1 and S2 of Supporting Information. Y.A. and E.V.L. thank SENESCYT (Secretaría Nacional de Educación Superior, Ciencia, Tecnología e Innovación) for allowing them the opportunity to participate in the Prometheus Program. They also gratefully acknowledge IVIC for the use of the computing facilities of the Laboratorio de Físico-Química Teórica de Materiales. The artwork was done by Mr. Alejandro Martínez.

REFERENCES

- (1) Weisser, O.; Landa, S. *Sulfide Catalysts: Their Properties and Application*; Pergamon Press: New York, 1973.
- (2) Hinnemann, B.; Moses, P. G.; Nørskov, J. K. Recent Density Functional Studies of Hydrodesulfurization Catalysts: Insight Into Structure and Mechanism. *J. Phys.: Condens. Mater.* **2008**, *20*, 064236.
- (3) Topsøe, H.; Clausen, B. S.; Massoth, F. E. Hydrotreating Catalysis. In *Catalysis, Science and Technology*; Springer: Berlin, 1996; Vol. 11, pp 1–269.
- (4) Chianelli, R. R.; Berhault, G.; Torres, B. Unsupported Transition Metal Sulfide Catalysts: 100 Years of Science and Application. *Catal. Today* **2009**, *147*, 275–286.
- (5) Eijsbouts, S.; Anderson, G.; Bergwerff, J.; Jacobi, S. Economic and Technical Impacts of Replacing Co and Ni Promotion in Hydrotreating Catalysts. *Appl. Catal., A* **2013**, *458*, 169–182.
- (6) Fontaine, C.; Romero, Y.; Daudin, A.; Devers, E.; Bouchy, C.; Brunet, S. Insight Into Sulphur Compounds and Promoter Effects on Molybdenum-based Catalysts for Selective HDS of FCC Gasoline. *Appl. Catal., A* **2010**, *388*, 188–195.
- (7) Ziolek, M. Niobium-containing Catalysts-The State of the Art. *Catal. Today* **2003**, *78*, 47–64.
- (8) Faro, A.; Dos Santos, A. Cumene Hydrocracking and Thiophene HDS on Niobia-supported Ni, Mo and Ni-Mo Catalysts. *Catal. Today* **2006**, *118*, 402–409.
- (9) Rocha, A. S.; Faro, A. C., Jr.; Oliviero, L.; Gestel, J. V.; Maugé, F. Alumina-, Niobia-, and Niobia/Alumina-supported NiMoS Catalysts: Surface Properties and Activities in the Hydrodesulfurization of Thiophene and Hydrodenitrogenation of 2,6-Dimethylaniline. *J. Catal.* **2007**, *252*, 321–334.

- (10) Afanasiev, P.; Bezverkhyy, I. Ternary Transition Metals Sulfides in Hydrotreating Catalysis. *Appl. Catal., A* **2007**, *322*, 129–141.
- (11) Danot, M.; Afonso, J.; Portefaix, J.; Breysse, M.; des Courieres, T. Catalytic Properties of Niobium Sulphides in the Conversion of Nitrogen Containing Molecules. *Catal. Today* **1991**, *10*, 629–643.
- (12) Gaborit, V.; Allali, N.; Geantet, C.; Breysse, M.; Vrinat, M.; Danot, M. Niobium Sulfide as a Dopant for Hydrotreating NiMo Catalysts. *Catal. Today* **2000**, *57*, 267–273.
- (13) Xiao, J.; Long, M.; Li, X.; Huang, H.; Gao, Y. Theoretical Prediction of Electronic Structure and Carrier Mobility in Single-walled MoS₂ Nanotubes. *Sci. Rep.* **2014**, *4*, 4327.
- (14) Ivanovskaya, V. V.; Zobelli, A.; Gloter, A.; Brun, N.; Serin, V.; Colliex, C. Ab Initio Study of Bilateral Doping within the MoS₂–NbS₂ System. *Phys. Rev. B: Condens. Matter Mater. Phys.* **2008**, *78*, 134104.
- (15) Wilson, J.; Yoffe, A. The Transition Metal Dichalcogenides Discussion and Interpretation of the Observed Optical, Electrical and Structural Properties. *Adv. Phys.* **1969**, *18*, 193–335.
- (16) Teer, D. New Solid Lubricant Coatings. *Wear* **2001**, *251*, 1068–1074.
- (17) Revenier, N. M.; Hampshire, J.; Fox, V. C.; Witts, J.; Allen, T.; Teer, D. Advantages of Using Self-lubricating, Hard, Wear-resistant MoS₂-based Coatings. *Surf. Coat. Technol.* **2001**, *142a*, 67–77.
- (18) *Intercalated Layered Materials*; Levy, F., Ed.; Physics and Chemistry of Materials with Layered Structure Series; Reidel Publishing Group: Dordrecht, The Netherlands, 1979; Vol. 6.
- (19) Afanasiev, P.; Fischer, L.; Beauchesne, F.; Danot, M.; Gaborit, V.; Breysse, M. Preparation of the Mixed Sulfide Nb₂Mo₃S₁₀ Catalyst from the Mixed Oxide Precursor. *Catal. Lett.* **2000**, *64*, 59–63.
- (20) Deepak, F. L.; Cohen, H.; Cohen, S.; Feldman, Y.; Popovitz-Biro, R.; Azulay, D.; Millo, O.; Tenne, R. Fullerene-Like (IF) Nb_xMo_{1-x}S₂ Nanoparticles. *J. Am. Chem. Soc.* **2007**, *129*, 12549–12562.
- (21) Ivanovskaya, V. V.; Heine, T.; Gemming, S.; Seifert, G. Structure, Stability and Electronic Properties of Composite Mo_{1-x}NbxS₂ Nanotubes. *Phys. Status Solidi B* **2006**, *243*, 1757–1764.
- (22) Raybaud, P.; Hafner, J.; Kresse, G.; Kasztelan, S.; Toulhoat, H. Ab Initio Study of the H₂-H₂S/MoS₂ Gas-Solid Interface: The Nature of the Catalytically Active Sites. *J. Catal.* **2000**, *189*, 129–146.
- (23) Schweiger, H.; Raybaud, P.; Kresse, G.; Toulhoat, H. Shape and Edge Sites Modifications of MoS₂ Catalytic Nanoparticles Induced by Working Conditions: A Theoretical Study. *J. Catal.* **2002**, *207*, 76–87.
- (24) Krebs, E.; Silvi, B.; Raybaud, P. Mixed Sites and Promoter Segregation: A DFT Study of the Manifestation of Le Chatelier's Principle for the Co(Ni)MoS Active Phase in Reaction Conditions. *Catal. Today* **2008**, *130*, 160–169.
- (25) Costa, D.; Arrouvel, C.; Breysse, M.; Toulhoat, H.; Raybaud, P. Edge Wetting Effects of γ-Al₂O₃ and Anatase-TiO₂ Supports by MoS₂ and CoMoS Active Phases: A DFT Study. *J. Catal.* **2007**, *246*, 325–343.
- (26) Arrouvel, C.; Breysse, M.; Toulhoat, H.; Raybaud, P. A Density Functional Theory Comparison of Anatase (TiO₂) and γ-Al₂O₃-supported MoS₂ Catalysts. *J. Catal.* **2005**, *232*, 161–178.
- (27) Reuter, K.; Stampfl, C.; Scheffler, M. Ab Initio Atomistic Thermodynamic and Statistical Mechanics of Surface Properties and Functions. In *Handbook of Materials Modeling*; Yip, S., Ed.; Springer: Dordrecht, The Netherlands, 2005.
- (28) Cristol, S.; Paul, J. F.; Payen, E.; Bougeard, D.; Clémendot, S.; Hutschka, F. Theoretical Study of the MoS₂ (100) Surface: A Chemical Potential Analysis of Sulfur and Hydrogen Coverage. *J. Phys. Chem. B* **2000**, *104*, 11220–11229.
- (29) Raybaud, P. Understanding and Predicting Improved Sulfide Catalysts: Insights from First Principles Modeling. *Appl. Catal., A* **2007**, *322*, 76–91.
- (30) Aray, Y.; Vega, D.; Rodriguez, J.; Vidal, A. B.; Grillo, M. E.; Coll, S. First-Principles Study of Low Miller Index Ni₃S₂ Surfaces in Hydrotreating Conditions. *J. Phys. Chem. B* **2009**, *113*, 3058–3070.
- (31) Aray, Y.; Vidal, A. B.; Rodriguez, J.; Grillo, M. E.; Vega, D.; Coll, D. S. First Principles Study of Low Miller Index RuS₂ Surfaces in Hydrotreating Conditions. *J. Phys. Chem. C* **2009**, *113*, 19545–19557.
- (32) Finnis, M. W. Accessing the Excess: An Atomistic Approach to Excesses at Planar Defects and Dislocations in Ordered Compounds. *Phys. Status Solidi A* **1998**, *166*, 397–416.
- (33) Reuter, K.; Scheffler, M. Composition, Structure, and Stability of RuO₂(110) as a Function of Oxygen Pressure. *Phys. Rev. B: Condens. Matter Mater. Phys.* **2001**, *63*, 035406.
- (34) Raybaud, P.; Costa, D.; Valero, M. C.; Arrouvel, C.; Digne, M.; Sautet, P.; Toulhoat, H. First Principles Surface Thermodynamics of Industrial Supported Catalysts in Working Conditions. *J. Phys.: Condens. Mater.* **2008**, *20*, 064235.
- (35) Rogal, J.; Reuter, K.; Scheffler, M. Thermodynamic Stability of PdO Surfaces. *Phys. Rev. B: Condens. Matter Mater. Phys.* **2004**, *69*, 075421.
- (36) Soon, A.; Todorova, M.; Delley, B.; Stampfl, C. Thermodynamic Stability and Structure of Copper Oxide Surfaces: A First-Principles Investigation. *Phys. Rev. B: Condens. Matter Mater. Phys.* **2007**, *75*, 125420.
- (37) Prodromme, P.-Y.; Raybaud, P.; Toulhoat, H. Free-energy Profiles Along Reduction Pathways of MoS₂ M-edge and S-edge by Dihydrogen: A First-Principles Study. *J. Catal.* **2011**, *280*, 178–195.
- (38) Accelrys; DMol³ is available as a part of Material Studio, 2009.
- (39) Delley, B. From Molecules to Solids with the DMol³ Approach. *J. Chem. Phys.* **2000**, *113*, 7756–7764.
- (40) Delley, B. An All-electron Numerical Method for Solving the Local Density Functional for Polyatomic Molecules. *J. Chem. Phys.* **1990**, *92*, 508–517.
- (41) Hägg, G.; Schönberg, N. *Ark. Kemi* **1954**, *7*, 371.
- (42) Perdew, J. P.; Burke, K.; Ernzerhof, M. Generalized Gradient Approximation Made Simple. *Phys. Rev. Lett.* **1996**, *77*, 3865–3868.
- (43) Aray, Y.; Rodríguez, J.; Vidal, A. B.; Coll, S. Nature of the NiMoS Catalyst Edge Sites: An Atom in Molecules Theory and Electrostatic Potential Studies. *J. Mol. Catal. A: Chem.* **2007**, *271*, 105–116.
- (44) Aray, Y.; Rodríguez, J. Atoms in Molecules Theory for Exploring the Nature of the MoS₂ Catalyst Edges Sites. *J. Mol. Catal. A: Chem.* **2007**, *265*, 32–41.
- (45) Silvi, B. The Spin-Pair Compositions as Local Indicators of the Nature of the Bonding. *J. Phys. Chem. A* **2003**, *107*, 3081–3085.
- (46) Becke, A. D.; Edgecombe, K. E. A simple measure of electron localization in atomic and molecular systems. *J. Chem. Phys.* **1990**, *92*, 5397–5403.
- (47) Bader, R. F. W. *Atoms in Molecules: A Quantum Theory*; Clarendon Press: Oxford, U.K., 1990.
- (48) Popelier, P. *Atoms in Molecules—An Introduction*; Prentice Hall: Harlow, England, 2000.
- (49) Gillespie, R.; Popelier, P. *Chemical Bonding and Molecular Geometry: From Lewis to Electron densities*; Oxford University Press: New York, 2001.
- (50) McDougal, J.; Hall, M. Study of Electron Distribution in Molecules and Crystal. *Trans. Am. Crystallogr. Assoc. (1965–1995)* **1990**, *26*.
- (51) Aray, Y.; Rodriguez, J.; Vega, D. Laplacian of the Electronic Charge Density and Heat of Adsorption of O₂ and CO Molecules on 3D Transition Metals. *J. Phys. Chem. B* **2000**, *104*, 5225–5231.